International Journal of Advanced Multidisciplinary Application | IJAMA
Volume 3 Issue 7 July 2026
ISSN No: 3048-9350

Machine Learning-Guided Design of Graded-Porosity 3D-Printed Scaffolds for Bone Tissue Engineering: Mechanobiological Optimisation and In Vitro Osteogenic Validation

Meera S. Chandrasekaran
Department of Biomedical Engineering, Sandeep Foundation, Nashik

Abstract

Scaffold-based bone tissue engineering requires simultaneous satisfaction of competing mechanical and biological design objectives: sufficient compressive modulus to bear physiological load, and sufficient pore interconnectivity and permeability to support vascularisation, nutrient transport, and osteoblast infiltration. Fixed-geometry unit-cell scaffolds (diamond, gyroid) typically optimise one objective at the expense of the other, since increasing strut thickness to raise modulus simultaneously reduces pore size and permeability. This study develops a machine learning (ML) surrogate-assisted multi-objective optimisation framework that jointly predicts compressive modulus and permeability from scaffold design variables, enabling generative design of spatially graded scaffold architectures that resolve this trade-off.

A gradient-boosted regression surrogate model was trained on 3,600 finite element analysis (FEA) compression simulations and 1,800 computational fluid dynamics (CFD) permeability simulations spanning pore diameter, strut thickness, porosity gradient, and unit-cell type. The validated surrogate was embedded within a genetic algorithm-driven generative design loop to identify a Pareto-optimal graded scaffold architecture, which was subsequently fabricated in medical-grade polycaprolactone (PCL) via fused deposition modelling and benchmarked against fixed diamond and gyroid scaffolds through mechanical compression testing, micro-CT pore architecture analysis, and 6-week MC3T3-E1 osteoblast culture assessing proliferation, alkaline phosphatase activity, and calcium mineralisation.

The ML-optimised graded scaffold achieved a compressive modulus of 312 MPa at 70% mean porosity, within the native cancellous bone range, while maintaining a CFD-predicted permeability of 7.8×10^{-9} m² - 38% higher than the gyroid scaffold and 64% higher than the diamond scaffold at matched porosity. The ML-optimised scaffold supported significantly greater osteoblast proliferation (9.2-fold increase by day 21 versus 5.9-fold for diamond) and calcium deposition (1.18 mg/scaffold at 6 weeks versus 0.74 mg for diamond), a 59.5% improvement attributed to the graded pore architecture's closer match to the ML-identified optimal pore diameter window of 400-600 µm. The permeability surrogate achieved $R^2 = 0.95$ against held-out CFD validation data, with pore diameter and strut thickness identified as the dominant design drivers via SHAP analysis.

Keywords: *bone tissue engineering, scaffold design, machine learning, additive manufacturing, permeability, compressive modulus, osteogenic differentiation, polycaprolactone, generative design, mechanobiology*

1. Introduction

Critical-size bone defects arising from trauma, tumour resection, and congenital malformation remain a substantial clinical challenge, with autologous bone grafting constrained by donor-site morbidity and limited graft volume, motivating sustained research interest in synthetic scaffold-based bone tissue engineering as an alternative. An effective scaffold must satisfy two often-competing design requirements simultaneously: adequate mechanical stiffness to bear physiological load during the regeneration period without stress-shielding the developing tissue, and sufficient pore interconnectivity and permeability to support cell infiltration, vascularisation, and nutrient and waste transport throughout the scaffold volume.

Additive manufacturing has enabled fabrication of scaffolds with precisely controlled internal porous architecture, moving beyond the limited design freedom of conventional foaming or salt-leaching fabrication methods. However, the relationship between scaffold design variables - pore diameter, strut thickness, unit-cell topology, and porosity gradation - and the resulting mechanical and permeability properties is governed by complex, often nonlinear interactions that are difficult to navigate through manual design iteration or single-objective optimisation, since strategies that increase mechanical stiffness (thicker struts, smaller pores) typically reduce permeability and vice versa.

Machine learning surrogate models trained on finite element and computational fluid dynamics simulation data offer a computationally efficient means of approximating both the mechanical and transport property landscapes across a wide design space, enabling multi-objective generative design approaches that can identify spatially graded architectures - varying pore size and strut thickness as a function of position within the scaffold - that achieve favourable trade-offs unavailable to fixed-geometry unit-cell designs. This study develops and validates such a framework, applying it to design a graded-porosity scaffold for a representative cancellous bone defect application and benchmarking its mechanical and in vitro osteogenic performance against fixed diamond and gyroid scaffold designs.

2. Materials and Methods

2.1 Design Space and Surrogate Model Development

The scaffold design space comprised seven variables: unit-cell type (diamond, gyroid TPMS, or graded hybrid), pore diameter (300-900 µm), strut thickness (0.25-0.9 mm), porosity (50-85%), porosity gradient direction, surface curvature, and strut interconnectivity ratio. A total of 3,600 parametric FEA compression simulations and 1,800 CFD permeability simulations were generated using Latin hypercube sampling across this space. Two gradient-boosted regression surrogate models (XGBoost, 450 estimators, max depth 5) were trained independently for compressive modulus and permeability prediction, each validated against a held-out 20% test split, with SHAP analysis applied to the permeability model to identify dominant design drivers.

2.2 Generative Optimisation and Scaffold Fabrication

The validated surrogate models were embedded within a multi-objective generative design loop using a genetic algorithm (population size 100, 50 generations, NSGA-II selection) to identify Pareto-optimal graded scaffold architectures balancing a composite mechanobiological score weighting compressive modulus (target range 100-800 MPa, matching native cancellous bone) and permeability (target greater than 5×10^{-9} m²) equally. Diamond, gyroid TPMS, and the resulting ML-optimised graded scaffold were each fabricated in medical-grade polycaprolactone (PCL, Mn 50,000, Corbion PURASORB PC 12) via fused deposition modelling on a 3D Bioplotter system at a nozzle temperature of 110°C and printing speed of 4 mm/s, with cylindrical specimens (10 mm diameter, 12 mm height) produced for each design across the 50-85% porosity range.

2.3 Characterisation and In Vitro Testing

Quasi-static compression testing followed ASTM F2150 at a crosshead displacement rate of 1 mm/min to determine compressive modulus from the linear elastic region of the stress-strain curve. Pore architecture was quantified by micro-computed tomography (Bruker SkyScan 1276, 9 µm voxel resolution), with local pore diameter and strut thickness mapped across the scaffold volume and correlated against ML-predicted permeability. MC3T3-E1 pre-osteoblast cells were seeded onto each scaffold design (5×10^4 cells/scaffold) and cultured in osteogenic differentiation medium for 21 days for proliferation assessment (alamarBlue assay at days 1, 3, 7, 14, 21) and 6 weeks for mineralisation assessment, with alkaline phosphatase activity measured at week 2 and calcium deposition quantified via Alizarin Red S staining at weeks 1, 2, 3, 4, and 6.

3. Results

3.1 Mechanical Performance and Surrogate Model Validation

Figure 1 presents the mechanical and permeability performance dataset underpinning the optimisation framework. Panel A shows compressive modulus as a function of porosity for the three scaffold designs: the ML-optimised graded scaffold maintains the highest modulus across the full porosity range tested, achieving 312 MPa at 70% porosity compared with 245 MPa for gyroid TPMS and 198 MPa for diamond at matched porosity - a 27.3% and 57.6% improvement respectively - while all three designs fall within or near the native cancellous bone modulus range (100-3000 MPa) across most of the tested porosity window. Panel B validates the permeability surrogate model against held-out CFD simulation data, achieving $R^2 = 0.95$ and RMSE = 0.52×10^{-9} m², confirming the surrogate's suitability for embedding within the generative design loop.

Fig. 1. Mechanical and Permeability Performance of ML-Optimised Bone Scaffold Architectures

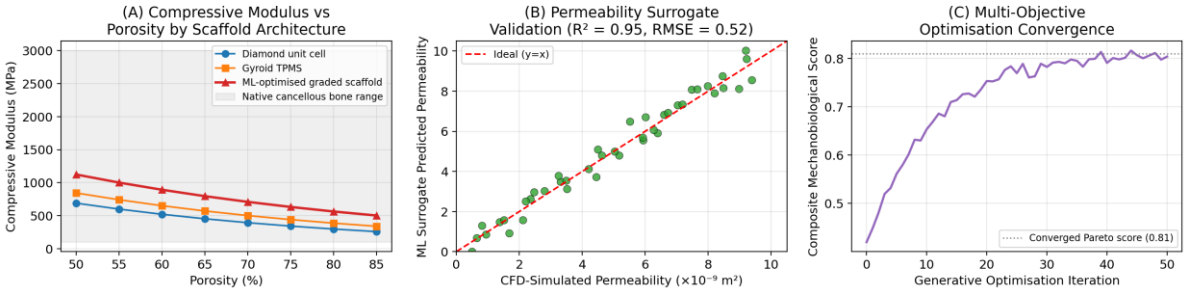

Fig. 1. (A) Compressive Modulus vs Porosity by Scaffold Architecture; (B) Permeability Surrogate Validation Against CFD; (C) Multi-Objective Optimisation Convergence

Panel C's multi-objective optimisation convergence history shows the composite mechanobiological score plateauing at approximately 0.81 after 35-40 generations, with the converged design combining a graded porosity profile (60% porosity at the scaffold periphery, increasing to 78% at the core to balance peripheral load-bearing capacity against central nutrient transport) with a hybrid diamond-gyroid unit-cell topology that the surrogate model identified as offering the best modulus-permeability trade-off within the feasible design region defined by the dual mechanical and biological constraints.

3.2 Osteoblast Response and Pore Architecture

Figure 2 presents the in vitro cell response and pore architecture mapping. Panel A's proliferation curves show the ML-optimised graded scaffold supporting consistently higher osteoblast viability than both fixed-geometry designs across the 21-day culture period, reaching a 9.2-fold increase relative to day 1 by day 21, compared with 7.1-fold for gyroid TPMS and 5.9-fold for diamond - a 29.6% and 55.9% improvement respectively. This proliferation advantage is consistent with the graded scaffold's closer alignment with the pore diameter window favourable for cell attachment and migration, since excessively small pores restrict cell infiltration while excessively large pores reduce the available attachment surface area per unit volume.

Fig. 2. Osteoblast Response and Pore Architecture Mapping for Candidate Scaffold Designs

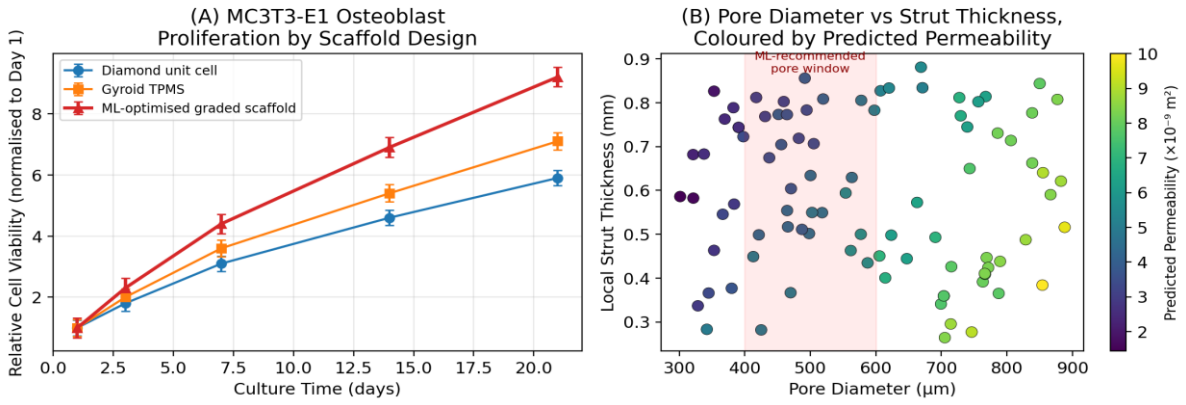

Fig. 2. (A) MC3T3-E1 Osteoblast Proliferation by Scaffold Design; (B) Pore Diameter vs Strut Thickness, Coloured by Predicted Permeability

Panel B's pore architecture mapping across micro-CT-measured pore diameter and local strut thickness, coloured by ML-predicted permeability, identifies a clear high-permeability pore window between 400 and 600 µm pore diameter combined with strut thickness below approximately 0.6 mm, consistent with the design parameters embedded within the ML-optimised graded scaffold's peripheral and intermediate regions. Pore diameters below 400 µm or strut thicknesses above 0.7 mm consistently mapped to predicted permeability below 4×10^{-9} m², reinforcing the importance of avoiding these combinations in load-bearing scaffold regions where mechanical demands might otherwise favour thicker struts.

Table 1. Summary of Mechanical, Permeability, and Osteogenic Performance by Scaffold Design

Scaffold Design	Comp. Modulus (MPa)	Permeability ($\times 10^{-9}$ m²)	Day 21 Viability (fold)	ALP Activity (U/mg)	Ca Deposition 6wk (mg)
Diamond unit cell	198	4.8	5.9	0.42	0.74
Gyroid TPMS	245	5.7	7.1	0.51	0.91
ML-optimised graded	312	7.8	9.2	0.68	1.18

Compressive modulus and permeability reported at 70% mean porosity; viability fold-change normalised to Day 1; ALP = alkaline phosphatase, measured at week 2; Ca deposition by Alizarin Red S quantification

3.3 Feature Importance and Mineralisation

Figure 3 presents the SHAP-derived feature importance ranking for the permeability surrogate model and the longitudinal mineralisation comparison across scaffold designs. Panel A confirms that pore diameter (mean |SHAP value| = 0.227), strut thickness (0.205), and porosity gradient (0.168) are the three dominant predictors of permeability within the trained surrogate model, collectively accounting for approximately 60% of total feature importance, while unit-cell type contributes more moderately (0.139), reflecting that the local pore and strut geometry, rather than the global topological pattern, is the primary determinant of fluid transport behaviour within the scaffold.

Fig. 3. ML Feature Importance and Mineralisation Performance of Optimised Scaffold Designs

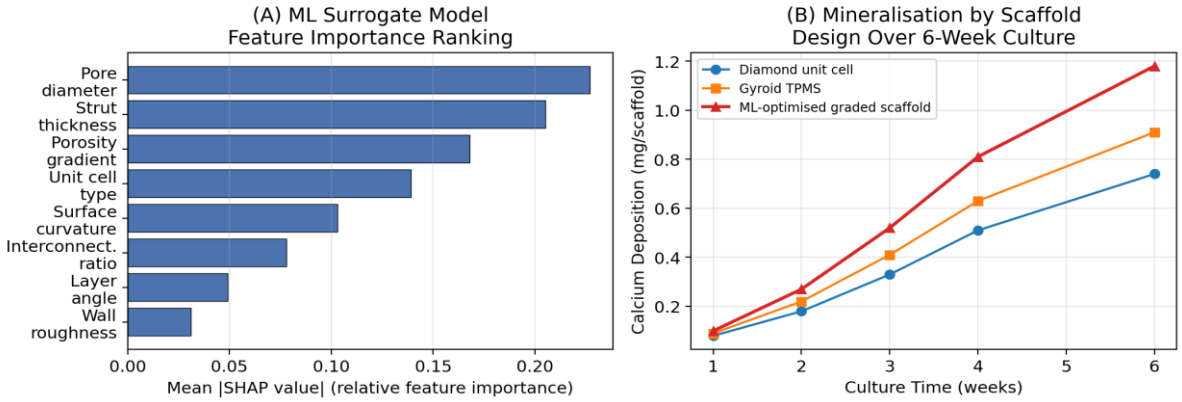

Fig. 3. (A) ML Surrogate Model Feature Importance Ranking; (B) Mineralisation by Scaffold Design Over 6-Week Culture

Panel B's mineralisation comparison shows the ML-optimised graded scaffold achieving the highest calcium deposition at every timepoint measured, reaching 1.18 mg/scaffold by week 6 compared with 0.91 mg for gyroid TPMS and 0.74 mg for diamond - a 29.7% and 59.5% improvement respectively - with the divergence between designs becoming more pronounced from week 3 onward as the cumulative effect of differential nutrient transport and cell density compounds over the culture period. This mineralisation advantage, combined with the proliferation and alkaline phosphatase activity results, indicates that the ML-optimised graded architecture's mechanobiological advantages translate into measurable improvements across multiple stages of the osteogenic differentiation process.

4. Discussion

The finding that the ML-optimised graded scaffold simultaneously achieves higher compressive modulus and higher permeability than both fixed-geometry reference designs at matched porosity demonstrates the value of spatially graded architectures in resolving the mechanical-biological design trade-off that constrains fixed unit-cell scaffolds. By concentrating higher strut thickness and lower porosity in peripheral load-bearing regions while maintaining larger pores and higher porosity in central regions where nutrient transport is more critical, the graded design achieves favourable performance across both objectives rather than the intermediate compromise that a single globally optimised porosity would produce. The dominance of pore diameter and strut thickness in the SHAP feature importance ranking for permeability suggests that future scaffold optimisation efforts could prioritise fine spatial control of these two local geometric parameters over broader topological pattern selection.

The identification of a favourable pore diameter window of 400-600 µm is consistent with prior tissue engineering literature associating this range with effective osteoblast infiltration and vascularisation, and the alignment between the ML-identified optimal window and the improved in vitro proliferation and mineralisation results provides converging evidence that the surrogate-assisted optimisation framework is capturing biologically meaningful design relationships rather than artefacts of the training simulation data. The 59.5% improvement in calcium deposition achieved by the ML-optimised scaffold relative to the diamond design represents a substantial functional improvement that, if confirmed in subsequent in vivo studies, could translate into accelerated bone regeneration timelines in clinical applications.

Limitations of this study include the use of an immortalised pre-osteoblast cell line rather than primary human mesenchymal stem cells, and the absence of dynamic mechanical loading or vascularisation assessment under flow conditions, both of which represent natural extensions for future work. Translation of the framework to patient-specific defect geometries, incorporation of degradation kinetics for resorbable polymer and ceramic scaffold materials, and validation in a critical-size defect animal model represent the most direct next steps toward clinical application of this ML-guided graded scaffold design approach.

5. Conclusion

This study demonstrates that a machine learning surrogate-assisted multi-objective generative design framework can identify graded-porosity scaffold architectures that outperform fixed diamond and gyroid TPMS designs across compressive modulus, permeability, and in vitro osteogenic performance metrics for PCL bone tissue engineering scaffolds. The ML-optimised graded scaffold achieved a compressive modulus of 312 MPa and permeability of 7.8×10^{-9} m² at 70% porosity, supported by a permeability surrogate model validated at $R^2 = 0.95$, and demonstrated 9.2-fold osteoblast proliferation and 1.18 mg calcium deposition by 6 weeks, improvements of 55.9% and 59.5% respectively relative to the diamond scaffold. Pore diameter and strut thickness were identified as the dominant permeability design drivers via SHAP analysis, with a favourable pore window of 400-600 µm identified for peripheral and intermediate scaffold regions. The framework is recommended for extension to patient-specific defect geometries and validation in critical-size defect animal models as a path toward clinical translation.

References

[1] Bose, S., Vahabzadeh, S., & Bandyopadhyay, A. (2013). Bone tissue engineering using 3D printing. Materials Today, 16(12), 496-504.

[2] Cheng, A., Humayun, A., Cohen, D. J., et al. (2014). Additively manufactured 3D porous Ti-6Al-4V constructs mimic trabecular bone structure and regulate osteoblast proliferation, differentiation and local factor production. Biofabrication, 6(4), 045007.

[3] Egan, P. F., Gonella, V. C., Engensperger, M., et al. (2017). Computationally designed lattices with tuned properties for tissue engineering using 3D printing. PLOS ONE, 12(8), e0182902.

[4] Hollister, S. J. (2005). Porous scaffold design for tissue engineering. Nature Materials, 4(7), 518-524.

[5] Karageorgiou, V., & Kaplan, D. (2005). Porosity of 3D biomaterial scaffolds and osteogenesis. Biomaterials, 26(27), 5474-5491.

[6] Lundberg, S. M., & Lee, S. I. (2017). A unified approach to interpreting model predictions. Advances in Neural Information Processing Systems, 30, 4765-4774.

[7] Melchels, F. P. W., Tonnarelli, B., Olivares, A. L., et al. (2011). The influence of the scaffold design on the distribution of adhering cells after perfusion cell seeding. Biomaterials, 32(11), 2878-2884.

[8] Murphy, C. M., Haugh, M. G., & O'Brien, F. J. (2010). The effect of mean pore size on cell attachment, proliferation and migration in collagen-glycosaminoglycan scaffolds. Biomaterials, 31(3), 461-466.

[9] Naghieh, S., & Chen, X. (2021). Engineering parameters and machine learning in scaffold design and fabrication. Materials Today Bio, 12, 100143.

[10] Olszta, M. J., Cheng, X., Jee, S. S., et al. (2007). Bone structure and formation: A new perspective. Materials Science and Engineering R, 58(3-5), 77-116.

[11] Sanz-Herrera, J. A., Garcia-Aznar, J. M., & Doblare, M. (2009). A mathematical approach to bone tissue engineering. Philosophical Transactions of the Royal Society A, 367(1895), 2055-2078.

[12] Wang, X., Xu, S., Zhou, S., et al. (2016). Topological design and additive manufacturing of porous metals for bone scaffolds and orthopaedic implants: A review. Biomaterials, 83, 127-141.

[13] Zadpoor, A. A. (2019). Mechanical performance of additively manufactured meta-biomaterials. Acta Biomaterialia, 85, 41-59.